Phe-NHMe and Ac-Tyr-Tyr-NHMe is required in order to explain the discrepancies encountered in these two cases.

Within these limits and for selected experimental cases, results of the present work support the hypothesis stated in the Introduction concerning the predictability of the side-chain conformational distribution for a given main-chain conformer without taking solvation into account. When, as in the case of Ac-Trp-Trp-NHMe dissolved in TFE, conformational freedom is reduced by lowering the temperature until only one or a few conformers contribute to the measured properties, it becomes possible to formulate a detailed model of these conformers. The two which best fit the ^{1}H NMR data are depicted in Figure 11. Although none of them is the lowest local minimum observed in the sector of the conformational space used to represent the folded form, they are found within 0.5 kcal/mol above this minimum and differ by about 0.1 kcal/mol from each other according to ECEPP. The geometry of the –Trp-Trp– fragment of conformer a_{II} is very similar to that already proposed for H-Trp-Trp-OH in alkaline methanol solution,[16] consistent with the similarities arising in the two cases.

A technical comment may be made about the comparison of the results obtained with the two different type of ensembles used to describe the side-chain conformational freedom. When the potential energy surface is constituted of shallow minima (as can be judged by the energy distribution of conformers sampled at random), the CD spectra calculated in either approximation coincide but the rotamer distribution appears to be more realistically smoothed in the Monte Carlo approximation (as in the cases of Ac-Phe-Phe-NHMe, Ac-Tyr-Tyr-NHMe, and of conformational state **b** of Ac-Trp-Trp-NHMe). On the contrary, for a steep minimum (Ac-Trp-Trp-NHMe in conformational state **a**) the two methods do not converge to the same result, probably because of the inefficiency of random sampling in such a situation.

The combination of experimental measurements with empirical calculations of molecular properties has proved to be essential for the conformational characterization of the systems investigated. It provides us with a simple interpretation of the observed conformational behavior of the side chains.

(a) The bulkiness of phenylalanine and tyrosine side chains appears to be limited enough so that in the corresponding dipeptides these are independent from each other whether the main chain is predominantly in an extended or in a folded conformer.

(b) With the more bulky tryptophan side chains, mutual influence limits their conformational freedom in the folded conformer of the main chain, where α substituents are on a same side, but not in an extended conformer of the main chain such as **b**, where α substituents are on opposite sides.

On the other hand, an explanation of the nature of the solvent effect on the conformation of the peptide main chain goes beyond the limits of the present study. As suggested by Madison and Kopple,[4] differential solvation of CO and NH groups may be one of the driving forces which establishes the conformational preferences of the peptide backbone in a protic solvent as opposed to a nonprotic solvent. A convincing test of this or other proposals has to wait for more numerous conformational studies of flexible peptides in solution.

Acknowledgment. We wish to thank Professor U. Suter for his generous assistance during the development, adapting, and debugging of computer programs in the preliminary phase of this work. We are grateful to B. Straub for her technical assistance with the CD measurements, to Dr. R. Keller, who kindly provided us with a subroutine for the calculation of ring-current effects, and to Dr. R. Thomas for his help with the editing of the manuscript. The stimulating criticism of Professor P. L. Luisi and Dr. G. P. Lorenzi is deeply appreciated.

Registry No. Ac-Trp-Trp-NHMe, 85702-36-9; Ac-Phe-Phe-NHMe, 53733-93-0; Ac-Tyr-Tyr-NHMe, 78582-82-8; Z-Phe-NHMe, 15368-72-6; Z-Tyr-NHMe, 20558-91-2; Z-Trp-NHMe, 53708-61-5.

Energy and Time Dependence of the Decay Processes of Toluene Molecular Cations

Rolf Bombach, Josef Dannacher, and Jean-Pierre Stadelmann*

Contribution from the Physikalisch-Chemisches Institut der Universität Basel, CH-4056 Basel, Switzerland. *Received January 17, 1983*

Abstract: The breakdown diagram of toluene cation has been determined by time-resolved He Iα photoelectron–photoion coincidence spectroscopy. Relying on a most recently developed procedure, the data have been analyzed within the framework of RRKM theory. The most notable outcomes concern: evidence for the entirely statistical nature of the investigated dissociative processes, the rate–energy functions for the formation of tropylium and benzylium cation, the 0 K enthalpies of formation of $\Delta H_f°_0$(tropylium cation) = 872 ± 6 kJ/mol and $\Delta H_f°_0$(benzylium cation) = 935 ± 9 kJ/mol, the rate-energy function for the secondary fragmentation of the $C_7H_7^+$ ions, an upper limit of $\Delta H_f°_0(C_5H_5^+)$ = 1034 ± 15 kJ/mol for the product ion of this latter reaction, and a quantitative determination of the considerable kinetic shift associated with this secondary process. The results are related to the earlier reported literature data stemming from a variety of experimental techniques. The present data agree essentially quantitatively with the outcome of a high-sensitivity photoionization study. The partly bimolecular character of ion cyclotron resonance and collisional activation data and the vastly unknown extent of the isomerization of the two isomeric $C_7H_7^+$ primary product ions prevent an extensive comparison with these results.

Introduction

The interpretation of the observed product ion distribution in terms of the structure of the ionized molecules represents a fundamental problem of organic mass spectrometry. To a certain extent, this can be paralleled with the classical chemical degradation technique, where the structure of a particular compound is also inferred from the nature of the products formed in the course of several specific decomposition reactions. However, it must be recalled that conventional mass spectrometry provides merely the mass to charge ratio (m/z) and the relative abundance of the fragment ions produced by a series of parallel and consecutive unimolecular reactions. The determination of the structures of these fragment ions and/or the details of the pathways for their formation is much more cumbersome and requires

0002-7863/83/1505-4205$01.50/0

Scheme I

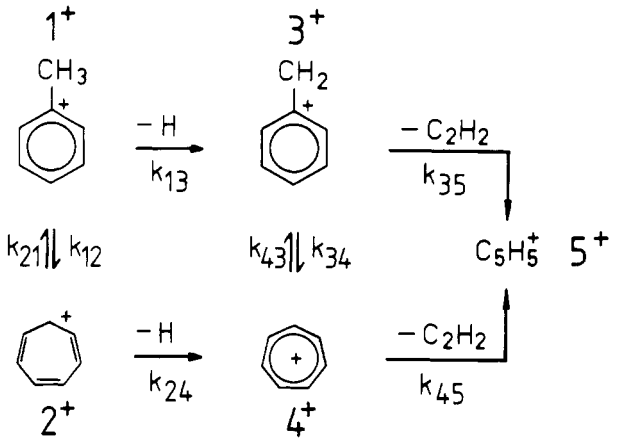

in general that more elaborate techniques are employed. A favorable way to gain such information relies on thermochemical data and on the outcomes of various experimental methods as, e.g., the study of metastable ions (MI), photoionization (PI), ion cyclotron resonance (ICR), photodissociation (PD), collisional activation (CA), and photoelectron–photoion coincidence (PEPICO) experiments. Furthermore, isotopic labeling and a study of substituent effects can be used to complete our knowledge.

During the last decade, much work has been devoted to elucidating the structure of $C_7H_7^+$, a dominant fragment ion in the mass spectra of various aromatic compounds. Clearly, the most carefully investigated precursor to $C_7H_7^+$ is toluene molecular cation ($\mathbf{1}^+$) which has been subject to all the above-mentioned techniques except for photoelectron–photoion coincidence spectroscopy. All earlier studies concur that the prevailing fragmentation reaction of excited toluene molecular cations

$$C_7H_8^+ \rightarrow C_7H_7^+ + H \qquad (1)$$

leads to at least two distinct structures of the $C_7H_7^+$ product ion. There is compelling evidence that the tropylium ($\mathbf{4}^+$) and the benzylium ($\mathbf{3}^+$) ions are involved, while the formation of further conceivable $C_7H_7^+$ isomers is significantly less well established. However, depending on the experimental technique used, strongly different values are reported for the relative amounts of $\mathbf{3}^+$ and $\mathbf{4}^+$ produced in the course of reaction 1. This may partly originate in the inherent properties of the various experiments, but is also a consequence of the distinct internal energy distributions of the sampled reactant and product ions as well as of the different time scales of the experiments. The formation of $\mathbf{3}^+$ and $\mathbf{4}^+$ through reaction 1 can unambiguously be quantified when the rate–energy functions of the unimolecular processes given in Scheme I are determined. Isotopic labeling,[1] ICR,[2,3] and CA data[4] suggest that reaction 1 is more endothermic than the first rearrangement process (Scheme I), which leads to a dynamic equilibrium between $\mathbf{1}^+$ and $\mathbf{2}^+$. The calculated activation energy of 165 kJ/mol[5] for the isomerization $\mathbf{1}^+ \rightarrow \mathbf{2}^+$ is in excellent agreement with a most recently reported experimental value of 159 kJ/mol,[6] obtained from matrix PI measurements. Referring to the statistical theory of unimolecular reactions,[7] the difference in activation energies and the properties of the transition state involved imply that k_{21} exceeds k_{12} by a few orders of magnitude at threshold, and that the ratio k_{12}/k_{21} decreases with increasing energy.

It is generally accepted that, close to the threshold energy of reaction 1, only the most stable $C_7H_7^+$ isomer, i.e., $\mathbf{4}^+$, can be formed. However, since the production of $\mathbf{4}^+$ from $\mathbf{1}^+$, which necessitates a rate-determining (preceding or concerted) ring expansion, represents a relatively slow fragmentation reaction, the higher energetic but more rapidly formed $\mathbf{3}^+$ becomes more and more the dominant product ion of reaction 1, if the excess energy of the precursor is increased. An additional aspect to be borne in mind, when the fractions of $\mathbf{3}^+$ and $\mathbf{4}^+$ are to be determined, concerns the isomerization of these two fragment ions. A recently calculated value, which is consistent with all the available experimental data, yields 137 kJ/mol[5] for the activation energy for the isomerization of $\mathbf{3}^+$ to $\mathbf{4}^+$. The relative stability of the two isomers implies that $\mathbf{3}^+$ isomerizes to $\mathbf{4}^+$ as soon as the internal energy of the former species suffices to surmount this energy barrier (i.e., $k_{34} > k_{43}$). Finally, the lowest energy secondary fragmentation

$$C_7H_7^+ \rightarrow C_5H_5^+ + C_2H_2 \qquad (2)$$

limits the maximum internal energy content of undissociated $C_7H_7^+$ ions to ~4 eV.

The exact determination of the threshold energy of reaction 1 is impeded by the presence of the expected kinetic shift, the extensive thermal excitation of the ionized toluene molecules at 300 K, and the fact that autoionization processes dominate the corresponding energy range. Time-resolved electron impact (EI) measurements[8] have provided evidence that an increase of the ion-trapping time from $\sim 10^{-6}$ to $\sim 10^{-3}$ s results in a displacement of the apparent threshold energy of reaction 1 from 11.9 to 10.7 eV. The latter value agrees quantitatively with the outcome of a PI study,[9] $AE(C_7H_7^+/\mathbf{1}; 298\ K) = 10.71 \pm 0.03$ eV, where a greatly increased sensitivity for ion detection helped to minimize kinetic shift effects. For obvious reasons, the threshold energy for $\mathbf{3}^+$ formation is even harder to establish. Probably the best estimate stems from PD measurements,[10] revealing that the onset for $\mathbf{3}^+$ production practically coincides with the spectroscopically determined photodissociation threshold. The relative amounts of $\mathbf{3}^+$ and $\mathbf{4}^+$ formed in the course of reaction 1 have been determined at internal energies of $\mathbf{1}^+$ where both product ions are energetically accessible, using PD,[10] ICR,[2] and CA[4] techniques. The reported values are in qualitative agreement as long as the estimated average internal energy of the generated $\mathbf{3}^+$ does not suffice for isomerization to $\mathbf{4}^+$. However, while the CA[4] data suggest that the fraction of $\mathbf{3}^+$ decreases above this isomerization threshold, reaching 30% at the highest energies investigated, the ICR[1] results in contrast imply that this fraction rises monotonously toward a high-energy asymptote of ~60%. Unfortunately, the internal energy distribution of the $C_7H_8^+$ precursor and of the $C_7H_7^+$ product ions remains unknown in the above-mentioned experiments, so that no definite conclusion can be drawn concerning the energetics and the energy dependence of the rate constants of the unimolecular processes involved.

The determination of the energy dependence of the unimolecular fragmentation rate constants has always been one of the most important objects in view of photoelectron–photoion coincidence spectroscopy. Following the first pioneering phase of this very powerful technique, time-resolved versions[11,12] of the experiment have lately been developed, which are particularly suited to study the fragmentation rates of internal energy selected molecular cations. Based on such experimental data, the statistical theory of unimolecular reactions could be tested stringently.[13] In several

(1) Howe, I.; McLafferty, F. W. *J. Am. Chem. Soc.* **1971**, *93*, 99.
(2) Jackson, J. A.; Lias, S. G.; Ausloos, P. *J. Am. Chem. Soc.* **1977**, *99*, 7515.
(3) Dunbar, R. C. *J. Am. Chem. Soc.* **1973**, *95*, 472.
(4) McLafferty, F. W.; Bockhoff, F. M. *J. Am. Chem. Soc.* **1979**, *101*, 1783.
(5) Dewar, M. J. S.; Landman, D. *J. Am. Chem. Soc.* **1977**, *99*, 2446. Cone, C.; Dewar, M. J. S.; Landman, D. *Ibid.* **1977**, *99*, 372.
(6) Andrews, L.; Keelan, B. W. *J. Am. Chem. Soc.* **1981**, *103*, 99.
(7) Forst, W. "Theory of Unimolecular Reactions"; Academic Press: New York, 1973.
(8) Gordon, S. M.; Reid, N. W. *Int. J. Mass Spectrom. Ion Phys.* **1975**, *18*, 379.
(9) Traeger, J. C.; McLoughlin, R. G. *J. Am. Chem. Soc.* **1977**, *99*, 7351. Traeger, J. C.; McLoughlin, R. G. *Int. J. Mass Spectrom. Ion Phys.* **1978**, *27*, 319.
(10) Dunbar, R. C. *J. Am. Chem. Soc.* **1975**, *97*, 1382.
(11) Stockbauer, R.; Rosenstock, H. M. *Int. J. Mass Spectrom. Ion Phys.* **1978**, *27*, 185.
(12) Dannacher, J.; Stadelmann, J.-P. *Chem. Phys.* **1980**, *48*, 79.
(13) Rosenstock, H. M.; Stockbauer, R.; Parr, A. C. *Int. J. Mass Spectrom. Ion Phys.* **1981**, *38*, 323.

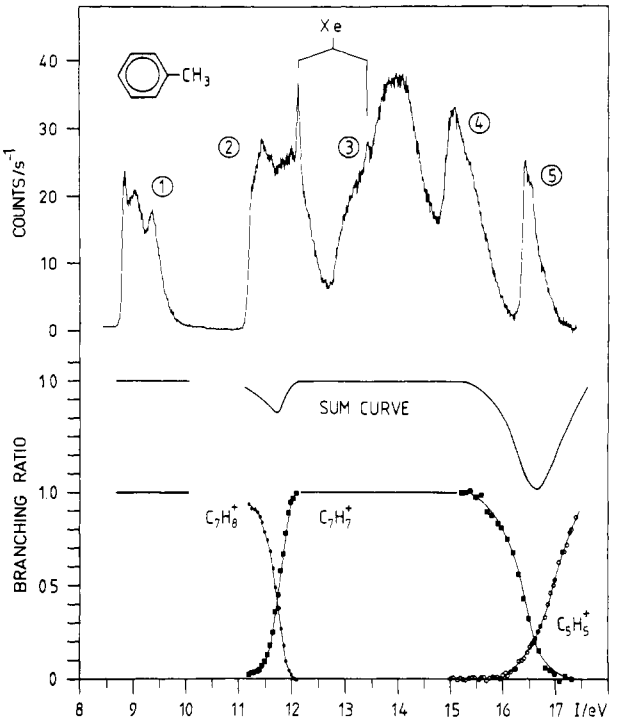

Figure 1. Photoelectron spectrum of toluene (top) and the breakdown diagram of its radical cation recorded at a sampling time of 45 μs.

instances, where the least endothermic fragmentation of the excited parent ion was clearly separated in energy from higher energetic processes, the statistical theory accounted very well for the experimental data, provided that reasonable values were selected for the activation energy and the frequencies of the reactant and of the transition state. A straightforward method to analyze the coincidence results by means of RRKM theory has been worked out and extensively tested on a large experimental data set gained for iodobenzene cation.[14] The degree of accord between theory and measurement was remarkable, particularly considering the fact that three distinct coincidence spectrometers had been employed covering a span of sampling times of two orders of magnitude. Most recently, the method has been elaborated,[15] aiming at an analysis of the clearly more important and more interesting cases of ionic dissociations where several fragmentations compete. Again, computed and measured rates were in close agreement and the calculated model functions accounted quantitatively for the measured breakdown diagram, even though numerous dissociation reactions and rather highly excited reactants ($E^* \approx 10$ eV) were involved.[16] The derived thermochemical quantities were in excellent agreement with the available literature data, though substantial competitive shift effects were operating.[16]

Referring to the present case, it is very plain that the determination of the rate–energy functions of two competing dissociations, leading to fragment ions of different structure but the same mass, represents a much more subtle problem, which can at best be solved in particularly favorable cases. In view of the above outlined picture on the decay of toluene cation, it could be surmised that the energy dependencies for the formation of 3^+ and 4^+ are sufficiently dissimilar, thus rendering possible such an analysis. Furthermore, reaction 2 provides an attractive example, where our approach can be applied for the first time to a secondary fragmentation of a primary daughter ion. Since the neutral fragment in reaction 1 is an atom, a determination of the kinetic energy release suffices to establish the energy content of

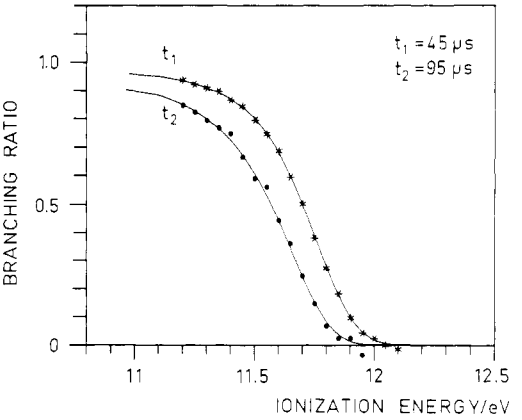

Figure 2. The decrease of the parent ion breakdown curve measured at 45 (*) and 95 (●) μs and calculated (solid lines) as described in the text.

Table I. Mass Spectral Data for Toluene

m/z	ion	PI, He Iα (21.22 eV)
92	$C_7H_8^+$	60
91	$C_7H_7^+$	100
90	$C_7H_6^+$	<0.5
89	$C_7H_5^+$	<0.5
66	$C_5H_6^+$	<0.5
65	$C_5H_5^+$	7
51	$C_4H_3^+$	<0.5
39	$C_3H_3^+$	<0.5

the subsequently decaying $C_7H_7^+$ daughter ions. The detailed analysis of the $C_7H_7^+$ breakdown curve yields also the critical energy for reaction 2 and, therefore, information about the structure of the corresponding reactant. The absence of any competing processes in the energy range of interest significantly facilitates the study of consecutive fragmentations in the case of toluene cation.

Experimental Section

The He Iα photoelectron–photoion coincidence spectrometer used in this study has previously[17] been described in detail. In brief, the sample gas effusing from a hypodermic needle is ionized by He Iα radiation ($h\nu$ = 21.22 eV). An electrostatic field of F_s = 2 V/cm is used to extract the ions, which are subsequently mass analyzed in a quadrupole mass spectrometer. The lapse of time between ion formation and ion detection can be varied by changing the axial pass energy and, hence, the residence time of the photoions in the mass filter. The transmission coefficient for molecular ions (m/z 92) was $f_i \approx 0.25$. The photoelectrons are energy analyzed by means of a hemispherical analyzer. An electron energy resolution of 75 meV (full width at half-maximum) was achieved and an extraordinarily high electron transmission coefficient of $f_e \approx 0.006$ was attained. The breakdown curves displayed in Figures 1 and 2 were obtained by scanning the photoelectron energy at a rate of ~1 eV/day. The electron energy was calibrated by adding small amounts of xenon to the toluene sample gas. The mass spectral intensities and the breakdown diagram have been corrected for ^{13}C isotope contribution. Commercially available toluene (Fluka AG, Buchs, Switzerland, stated purity >99.9%) was used without further purification. No significant traces of impurities could be detected in the course of the present study.

Results and Discussion

The PE spectrum of toluene recorded under the above-given experimental conditions is presented in Figure 1. According to ref 18, each of the two lowest energetic bands is due to electrons stemming from two distinct molecular orbitals (circled 1: $\pi(b_1)$, $\pi(a_2)$; circled 2: σ, $\pi(b_1)$). A detailed assignment of bands (circled 3, 4, and 5) has not yet been proposed. The fragmentation behavior of the generated photoions is remarkably simple, as the mass spectral data collected in Table I demonstrate. The mo-

(14) Dannacher, J.; Rosenstock, H. M.; Buff, R.; Parr, A. C.; Stockbauer, R. L.; Bombach, R.; Stadelmann, J.-P. *Chem. Phys.* **1983**, *75*, 23.
(15) Bombach, R.; Dannacher, J.; Stadelmann, J.-P. *J. Am. Chem. Soc.* **1983**, *105*, 1824.
(16) Bombach, R.; Dannacher, J.; Stadelmann, J.-P.; Neier, R. *Helv. Chim. Acta* **1983**, *66*, 701.
(17) Bombach, R.; Schmelzer, A.; Stadelmann, J.-P. *Int. J. Mass Spectrom. Ion Phys.* **1982**, *43*, 211.
(18) Debies, T. P.; Rabalais, J. W. *J. Electron Spectrosc. Relat. Phenom.* **1972**, *1*, 355.

lecular ion and the only two significant fragment ions, i.e., $C_7H_7^+$ and $C_5H_5^+$, account for 99% of the total ionization cross section for He Iα resonance radiation.

The breakdown diagram depicted in Figure 1 provides detailed information on the energy dependence of the fragmentation reactions involved. The parent ion branching ratio is unity within the energy range of PE band (circled 1), indicating that all toluene cations which are initially formed in their electronic ground state or in their first excited electronic state are detected undissociated. Referring to the sampling function and the time scale of our experiment, the parent ion breakdown curve begins to decrease at the onset of PE band (circled 2) and vanishes above $I > 12$ eV. The simultaneously rising $C_7H_7^+$ breakdown curve, which assumes a value of unity at 12 eV $< I <$ 16 eV, identifies reaction 1 as the only significant fragmentation channel in this energy range. At $I > 16$ eV, a decrease of the $C_7H_7^+$ breakdown curve sets in and the $C_5H_5^+$ breakdown curve starts to rise. Respecting also the behavior of the sum curve, the coincidence data point at a secondary fragmentation of the sufficiently excited $C_7H_7^+$ first generation daughter ions by loss of an acetylene molecule, i.e., reaction 2, and rule out a conceivable competitive decay of $\mathbf{1}^+$ according to the reaction:

$$C_7H_8^+ \rightarrow C_5H_5^+ + C_2H_3 \qquad (3)$$

The fixed wavelength coincidence experiment employed in the present study renders it possible to establish unambiguously the transmission coefficient for thermal parent ions.[17] Since this quantity is independent of the internal energy content of the molecular ions probed, the fraction of molecular ions with lifetimes longer than the experimental sampling time can be precisely determined as a function of the imparted energy. In general, a comparably accurate quantification of fragment ions is much more arduous, because their transmission coefficient is no longer a constant but depends on their kinetic energy, which in its turn commonly rises with increasing excess energy of the precursor. Moreover, the transmission coefficient for fragment ions is also reduced when slowly fragmenting molecular ions dissociate outside the ion source, so that the corresponding product ions escape detection for experimental reasons. Emerging exclusively in the threshold region of a particular fragmentation, the latter effect results in local dips of the sum curve (Figure 1), while monotonously decreasing sum curves are observed when the transmission coefficient is predominantly reduced owing to high kinetic energy fragment ions. In the present case, the two local minima of the sum curve originate unequivocally in the relatively small values of the unimolecular rate constants of reactions 1 and 2 in the corresponding threshold regions.

In order to derive the rate–energy function of reaction 1, the breakdown curve of the toluene molecular cation has precisely been determined in the relevant energy range (Figure 2). The significant shift of the breakdown curve to lower energies which accompanies an increase of the experimental sampling time from 45 to 95 μs clearly indicates the presence of slowly fragmenting molecular ions. In the first instance, the experimental data were assigned to one single unimolecular fragmentation and analyzed as follows. The energy-dependent rate constant k was calculated from[7]

$$k(E^* - E_0) = \sigma\, W^*(E^* - E_0)/h\rho(E^*) \qquad (4)$$

where E^*, E_0, σ, $W^*(E^* - E_0)$, $\rho(E^*)$, and h denote the internal energy of the reactant, the critical energy of the process, the reaction path degeneracy, the integrated density of states of the transition state at $(E^* - E_0)$, the density of states of the reactant at E^*, and Plank's constant, respectively. The molecular parameters of neutral toluene[19] have been used to characterize the reactant. The internal rotation of the methyl group and diverse C–H vibrations have been tried as reaction coordinates. The molecular frequencies of toluene multiplied by a constant factor F were employed to describe the transition state. Using E_0 and

(19) Sverdlov, L. M.; Kovner, M. A.; Krainov, E. P. "Vibrational Spectra of Polyatomic Molecules"; Wiley: New York, 1977.

Table II. Parameters, Obtained from the RRKM Analysis of Coincidence Data

reaction	ionic fragment	t/μs	E_0/eV	F	AE_0/eV
1	4^+	45	1.704 ± 0.063	1.64 ± 0.16	10.52 ± 0.07[a]
1	4^+	95	1.696 ± 0.116	1.63 ± 0.37	
1	3^+	45	2.351 ± 0.046	0.94 ± 0.07	11.17 ± 0.10[a]
1	3^+	95	2.351 ± 0.187	0.93 ± 0.18	
2	5^+	25	3.97 ± 0.08	0.90 ± 0.03	
2	5^+	45	4.02 ± 0.08	0.90 ± 0.02	14.55 ± 0.15[b]
2	5^+	95	4.04 ± 0.07	0.91 ± 0.03	

[a] 0 K appearance energy, the sum of E_0 and the first adiabatic ionization energy of **1**. [b] 0 K appearance energy, the sum of E_0 and $AE_0(4^+/1) = 10.52 \pm 0.07$ eV.

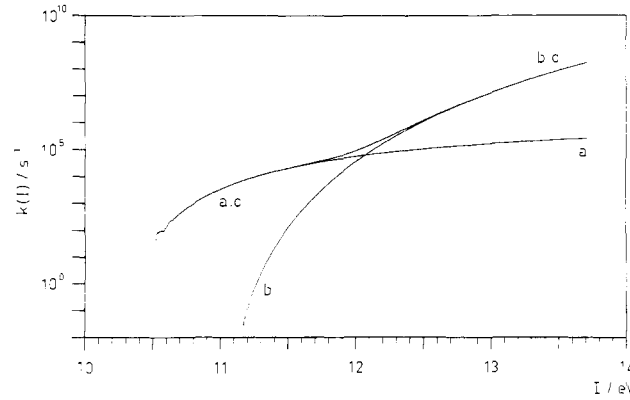

Figure 3. The total rate–energy function (c) for $C_7H_7^+$ formation and the individual rate–energy functions for tropylium (a) and benzylium (b) ion production.

F as adjustable parameters and taking carefully into account the effective sampling function of the experiment (which contains the vibrational and rotational thermal excitation of the ionized molecules, the transmission function of the electron energy analyzer, and the Franck–Condon envelope for He Iα photoionization), calculated breakdown curves were fit to both sets of experimental data points. Although this method has been proven to be highly reliable,[14,15] the achieved degree of accord between measured and calculated values was rather poor in the present case. Values of E_0 and F which led to agreement between computed and measured data in the low-energy section failed to account for the more steeply declining experimental breakdown curve at higher energies, and vice versa. Moreover, as a quantitative description of the observed time dependence could not be attained, the model had to be discarded.

Relying on the quoted results of independent previous research, the coincidence data were analyzed in a second way based on two competitive unimolecular reactions, which happen to produce fragment ions of identical mass to charge ratio. In the case of the less endothermic fragmentation with $\mathbf{4}^+$ as the charged product, a reaction path degeneracy of $\sigma = 6$ was employed and the internal rotation of the methyl group was chosen to represent the reaction coordinate. The analogous quantities of $\mathbf{3}^+$ formation were $\sigma = 3$ and a C–H stretching mode. The rates of both processes were then calculated according to (4), summed up to yield the total fragmentation rate of the molecular ion, converted into a breakdown curve as previously explained, and fit separately to the two independent data sets, using two critical energies and two frequency multiplicators as adjustable parameters. Within the rather small limits of error, identical values for these parameters (Table II) were derived from the two data sets. Excellent agreement between computed and measured values is obtained, in particular, for the more precisely determined short time data (Figure 2). The corresponding rate–energy functions depicted in Figure 3 characterize reaction 1 in a comprehensive manner. The deduced enthalpies of formation for $\mathbf{3}^+$ and $\mathbf{4}^+$ are in very good accord with independent literature values (Table III). Note

Table III. Relevant Thermochemical Data[a]

	neutral		cation		
	$\Delta H_f^\circ{}_0$(g) (kJ/mol)	$\Delta H_f^\circ{}_{298}$(g) (kJ/mol)	ionization energy (eV)	$\Delta H_f^\circ{}_0$(g) (kJ/mol)	$\Delta H_f^\circ{}_{298}$(g) (kJ/mol)
C_7H_8, **1**	73.3[b]	50.00	8.82 ± 0.01	924. ± 1[c]	901. ± 1
C_7H_8, **2**	203.8[d]	181.88	8.29 ± 0.01[e]	1004. ± 1[c]	982. ± 1
C_7H_7, **3**	219. ± 6[c]	200. ± 6[f]	7.20 ± 0.02[g]	914. ± 7[c]	895. ± 7
	240. ± 10			935. ± 9[h]	
C_7H_7, **4**	275. ± 8[c]	257. ± 8	6.24 ± 0.01	877. ± 8[c]	859. ± 8[i]
	270. ± 6			872. ± 6[j]	
C_5H_5, **5**				1013. ± 21[c]	1000. ± 21[k]
				1034. ± 15[l]	
C_2H_2	227.292	226.73			
	216.003	217.965			

[a] Data drawn from ref 26 in the absence of other citations. [b] Conversion of the corresponding room-temperature value to 0 K using the vibrational frequencies given in ref 19 and the approximate enthalpy function of ref 27. [c] Estimated from the corresponding room-temperature value. [d] Conversion of the corresponding room-temperature value to 0 K using the vibrational frequencies given in ref 28 and the approximate enthalpy function of ref 27. [e] Reference 9. [f] Reference 29. [g] Reference 30. [h] This work, calculated according to $\Delta H_f^\circ{}_0$(g)-($3^+/1$) = $AE_0(3^+/1) + \Delta H_f^\circ{}_{0(g)}(1) - \Delta H_f^\circ{}_{0(g)}$(H). [i] Reference 31. [j] This work, calculated according to $\Delta H_f^\circ{}_{0(g)}(4^+/1) = AE_0(4^+/1) + \Delta H_f^\circ{}_{0(g)}(1) - \Delta H_f^\circ{}_0$(H). [k] Reference 23. [l] This work, calculated according to $\Delta H_f^\circ{}_{0(g)}(5^+/1) = AE_0(5^+/1) + \Delta H_f^\circ{}_{0(g)}(1) - \Delta H_f^\circ{}_{0(g)}$(H) - $\Delta H_f^\circ{}_{0(g)}(C_2H_2)$.

that any direct experimental determination of the respective threshold energies will be impeded by kinetic and competitive shift effects, as well as by the mutual position of the dissociation limits and the populated electronic states of toluene cation. Production of $\mathbf{3}^+$ is evidently (Figure 3) the only primary process above I = 12.3 eV, while $\mathbf{4}^+$ formation prevails at lower energies. Therefore, apart from contributions from isomerizing $\mathbf{3}^+$, the detected $\mathbf{4}^+$ stem predominantly from $\mathbf{1}^+$ initially formed in their second or third excited electronic state (PE band, circled 2). The originally even higher excited molecular ions yield practically exclusively $\mathbf{3}^+$ which may subsequently isomerize and/or fragment further according to (2). The extent of this isomerization cannot be probed directly by the present coincidence technique, but an appropriate rate–energy function for the secondary fragmentation (eq 2) can be worked out.

RRKM theory[7] asserts that there is no fundamental difference between a primary fragmentation of an excited molecular cation and a secondary decay of a particular first generation daughter ion. However, in practice the latter case is more involved inasmuch as it is additionally necessary to assess the fraction of the excess energy of the primary process which is retained by the first generation daughter ion and, hence, available for a subsequent dissociation. Considering simply average energies is clearly insufficient as large fluctuations emerge, resulting in a pronounced broadening of the effective sampling function for the secondary process. When the neutral fragment of the primary dissociation is merely an atom, the available excess energy is partitioned among the internal degrees of freedom of the product ion and the external degrees of freedom of the separating fragments. Neglecting extensive excitation of external rotations, the required distribution of the excess energy can be gained, provided that the distribution of the released kinetic energy can be established.

Referring to the most general case, neither the theoretical nor the experimental means are currently available in order to solve this latter problem rigorously. This applies also to photoelectron–photoion coincidence spectroscopy which can be employed to quantify the distribution of released kinetic energies and its dependence on the available excess energy, when small ($n \leq 4$) molecular ions are probed,[20] where the vibrational levels of the fragment ions are sufficiently coarsely spaced; thus, the corresponding data analysis is feasible. In the case of larger ions, merely the average kinetic energy of the fragment ions can be deduced from the coincidence signal. Our present results imply that a constant average fraction of ~10% of the available excess energy of reaction 1 is converted into translational energy of the fragments. This value can only serve as an estimate inasmuch as the kinetic energy of the ionic fragment, i.e., the actually measurable quantity, represents only 1% of the total energy released. Therefore, the apparent broadening of the $C_7H_7^+$ time-of-flight distributions is very small, resulting in very large errors in the total kinetic energy release calculated from them. By comparison, relying on a frequently used empirical relationship,[21] a kinetic energy release of ~6% of the excess energy is expected.

Assuming that the released kinetic energy originates exclusively from statistical energy partitioning of the available excess energy between the internal degrees of freedom of the transition state and the reaction coordinate, the resulting distribution can be obtained from the statistical theory of unimolecular reactions.[22] The average translational energies derived from such calculations are always smaller than the corresponding experimental values.[7] Nevertheless, since sufficiently accurate experimental data are lacking, we rely on such a simple statistical account of the translational energy distribution, yielding an average kinetic energy of ~3% of the excess energy of reaction 1. Accordingly, the inferred effective sampling function of the secondary process presumably contains only a lower bound for the translational energy released in the course of the primary reaction 1.

Comparison of three independent data sets obtained at sampling times of 25, 45, and 95 μs reveals clearly that the declining section of the $C_7H_7^+$ breakdown curve (Figure 1) is displaced to higher energies when the period of time between ion formation and ion detection is shortened. Therefore, the $C_7H_7^+$ ions involved must have dissociative lifetimes comparable to these experimental time scales. Allowing for the kinetic energy release of reaction 1, as outlined in the preceding paragraph, the internal energy distribution of the $C_7H_7^+$ ion can be worked out and the rate–energy function for (2) can be determined, relying essentially on the same procedure as applied in the case of reaction 1. A single fragmentation (eq 2) was considered, leading to only one product ion structure $\mathbf{5}^+$, with $\mathbf{4}^+$ as reactant and $\sigma = 7/2$. The values for the critical energy E_0 and the transition-state frequency multiplier F obtained from independent fits to the three experimental data sets differ somewhat as Table II shows. These differences are primarily a consequence of the practically vanishing Franck–Condon factor around I = 16 eV and above I = 17 eV (Figure 1). Extremely low photoelectron intensities substantially reduce the attainable signal-to-noise ratio of the coincidence data. Therefore, the larger the portion of the descent of the $C_7H_7^+$ breakdown curve which is located at ionization energies with low photoelectron count rates, the smaller the accuracy of the measured data. Since the 25-μs data set is particularly degraded by this effect, the values for E_0 and F derived from the measurements at 45 and 95 μs and the corresponding rate–energy functions (Figure 4) are more reliable. An average enthalpy of formation

(20) Bombach, R.; Dannacher, J.; Stadelmann, J.-P.; Lorquet, J. C. *J. Chem. Phys.*, in press.

(21) Haney, M. A.; Franklin, J. L. *J. Chem. Phys.* **1968**, *48*, 4093.
(22) Taubert, R. *Z. Naturforsch. A.* **1964**, *19*, 911.

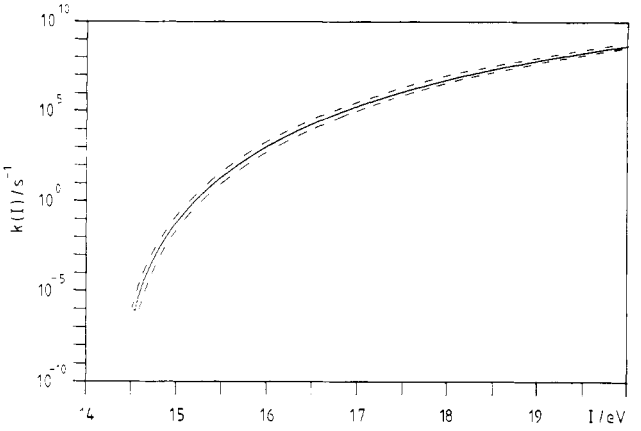

Figure 4. The rate–energy functions for the secondary fragmentation of $C_7H_7^+$ into $C_5H_5^+$ as derived from three independent breakdown curves recorded at 25 (top), 45 (middle), and 95 (lower) μs.

for the $C_5H_5^+$ fragment ions of $\Delta H_f°_0(C_5H_5^+)$ = 1034 ± 15 kJ/mol is derived from these two data sets. Since only a lower limit for the kinetic energy release of reaction 1 was taken into account in the analysis of the coincidence data for reaction 2 (see above), our value represents merely an upper limit which compares favorably with an independently determined upper bound of $\Delta H_f°_{298}(C_5H_5^+)$ = 1000 ± 21 kJ/mol.[23]

The entire analysis for the secondary fragmentation (eq 2) has been repeated adopting $\mathbf{3}^+$ as precursor structure. Within the limits of error the same $\Delta H_f°_0(C_5H_5^+)$ was derived, while a significantly larger F value of ~1.07 was obtained. This implies a modestly tight transition state for acetylene loss from $\mathbf{3}^+$, in contrast to a rather loose activated complex relative to a $\mathbf{4}^+$ structure of the precursor, characterized by $F \approx 0.9$ (Table II). A definite conclusion about the structure(s) of the dissociating reactant(s) can unfortunately not be made, based on our analysis of the declining $C_7H_7^+$ breakdown curve.

Conclusions

The fragmentation pathways of internal energy selected toluene cations have been established, employing time-resolved photoelectron–photoion coincidence spectroscopy and a detailed RRKM analysis of the corresponding experimental data. The parent ion is involved in solely two primary dissociations which happen to yield isomeric $C_7H_7^+$ fragment ions. Statistical theory accounts quantitatively for the breakdown curves and their dependence on the sampling time, provided that two competitive unimolecular reactions leading to two structurally distinct $C_7H_7^+$ fragment ions are explicitly considered. Following the extensive literature available, the more stable $C_7H_7^+$ species can be identified with the tropylium ion ($\mathbf{4}^+$), whereas the benzylium ion structure ($\mathbf{3}^+$) can be ascribed to the higher energy isomer. The present work provides the rate–energy functions and, hence, also the critical energies for the production of both isomers. The deduced 0 K threshold energy for $\mathbf{4}^+$ formation agrees within the given limits of error with the outcome of a time-resolved EI study[8] and the results of high sensitivity PI work.[9] The derived 0 K threshold energy for $\mathbf{3}^+$ production coincides practically with the onset energy of the second PE band, as had previously been inferred from PD experiments.[10] The rate–energy functions reveal clearly that H abstraction from toluene cation becomes more and more a kinetically controlled dissociation when the internal energy of the reactant is gradually increased. Our analysis indicates further that the electronic excess energy of the initially generated toluene ions is rapidly converted into vibrational energy of the electronic ground state, where the rate-determining steps for the formation of the two isomeric $C_7H_7^+$ ions compete effectively. Because of its comparatively low critical energy and its quickly rising rate–energy function, the formation of $\mathbf{3}^+$ quenches the production of other conceivable primary fragment ions, as e.g., $C_6H_5^+$ or $C_5H_5^+$.

(23) McCrery, D. A.; Freiser, B. S. *J. Am. Chem. Soc.* **1978**, *100*, 2902.

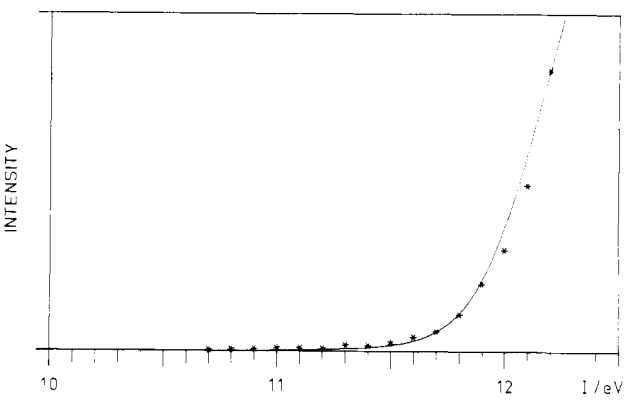

Figure 5. PI efficiency curve for $C_7H_7^+$ redrawn from ref 9 (*) and calculated from the coincidence data assuming an ion source residence time of 3 μs (solid line).

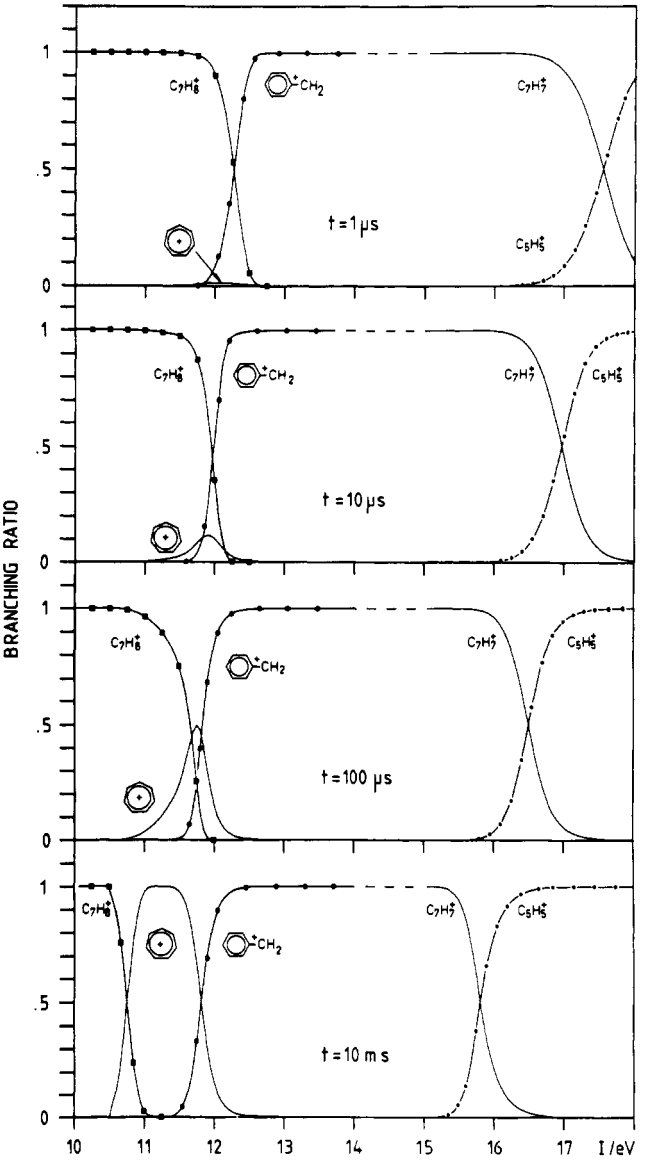

Figure 6. Dependence of the 0 K breakdown diagram on the indicated time scale. Note that the kinetic energy release of the primary process has been considered as outlined in the text, in order to derive the 0 K breakdown curve for the secondary process.

A conventional PI efficiency curve for a particular m/z value conforms to the integrated coincidence curve, if a step function threshold law may be assumed.[26] Therefore, based on the total rate for $C_7H_7^+$ production, the present coincidence results can be compared with the reported PI data[9] at all ionization energies

where electronic states of the toluene molecular cation can be populated by direct He Iα photoionization. Allowing for the initial thermal internal energy distribution of the photoionized toluene molecules, integrated coincidence curves have been computed for a few selected values of the source residence time. The highest energy point of the PI data[9] has been used to scale the integrated coincidence curves. The computed functions agree very well with the reported PI data for residence times between 1 and 5 μs, as the example presented in Figure 5 evidences. However, the substantial change of the slope at $I \simeq 10.7$ eV (Figure 5) is not related to the nature of the initially populated electronic states as had been proposed,[9] but originates exclusively in the behavior of the total rate–energy function, which begins to be influenced by the formation of the kinetically controlled product ion ($\mathbf{3}^+$) at this energy.

The comparison of our results with the outcomes of the ICR[2] and CA[4] studies is, unfortunately, less straightforward because bimolecular processes also occur in these experiments and subsequent isomerizations and fragmentations of the primary product ions must be taken into account. The consecutive decay of toluene cation to $C_7H_7^+$ and then to $C_5H_5^+$ has been established by MI experiments,[24] many years ago. The present study demonstrates that this is the only accessible pathway for $C_5H_5^+$ production. The detailed analysis of the coincidence data for this secondary reaction has provided the rate–energy function and an upper bound for the enthalpy of formation of the $C_5H_5^+$ product ion. The determined kinetic shift on the order of 1 eV which is associated with the acetylene loss from $C_7H_7^+$ is consistent with the statistical nature of this process and compares favorably with the corresponding kinetic shift for the lowest energy fragmentation of benzene cation, involving a precursor of similar size and a comparable activation energy. However, the structure of the dissociating $C_7H_7^+$ ions could not be inferred from the coincidence data.

At present, the equilibrium between $\mathbf{3}^+$ and $\mathbf{4}^+$ can only be characterized in a qualitative way. Relying on the statistical theory of unimolecular reactions, it can be expected that, close to the isomerization threshold, the prevailing primary product ion structure $\mathbf{3}^+$ will isomerize relatively slowly to $\mathbf{4}^+$ and that the reverse process can be neglected completely. It is conceivable that the relative stability of the two isomers (which favors $\mathbf{4}^+$ as product) ceases to dominate at higher excitation energies, inasmuch as interconversion of $\mathbf{3}^+$ to $\mathbf{4}^+$ involves a tighter transition state than the reverse reaction. Referring to classical terms, a larger preexponential factor might balance or even overcompensate the energetic aspect. It is well possible that the complex energy and time dependence of this $\mathbf{3}^+ \rightleftharpoons \mathbf{4}^+$ equilibrium is responsible for the disagreement between ICR[2] and CA data,[4] which appears to persist according to most recently reported results.[25] However, the results of the present study can be used to determine unambiguously the fractions of $\mathbf{3}^+$ and $\mathbf{4}^+$ formed by unimolecular dissociations of toluene molecular cation, provided that the initially generated internal energy distribution of the parent ions, the sampling function, and the time scale of the technique relied on are sufficiently precisely known. As an illustration, the 0 K breakdown diagram has been calculated for a few selected sampling times (Figure 6). Evidently, the most striking feature concerns the dependence of the probability for $\mathbf{4}^+$ formation on the experimental time scale. While the corresponding "high-energy cutoff" is completely determined by the rate of the competitive $\mathbf{3}^+$ formation, a considerable reduction of the apparent onset energy accompanies a significant extension of the time scale by four orders of magnitude. Apart from this dramatic time dependence, the actually detected fraction of $\mathbf{4}^+$ depends also on the strongly varying ionization cross section in this ionization energy range. It can be concluded that the present approach is a very powerful probe to quantify the unimolecular fragmentation processes of internal energy selected radical cations.

Acknowledgment. This work is part C28 of Project No. 2.017–081 of the Schweizerischer Nationalfonds zur Förderung der Wissenschaftlichen Forschung (part C27, ref 32). Financial support by the Max Geldner-Stiftung, Ciba-Geigy SA, F. Hoffmann-La Roche & Cie SA, and Sandoz SA (Basel) is gratefully acknowledged.

Registry No. Toluene, 108-88-3; toluene cation, 34504-47-7; benzylium cation, 6711-19-9; tropylium cation, 26811-28-9.

(24) Jennings, K. R.; Futrell, J. H. *J. Chem. Phys.* **1966**, *44*, 4315.
(25) Ausloos, P. *J. Am. Chem. Soc.* **1982**, *104*, 5259.
(26) Rosenstock, H. M.; Draxl, K.; Steiner, B. W.; Herron, J. T. *J. Phys. Chem. Ref. Data Suppl. 1* **1977**, *6*.
(27) Stull, D. R.; Prophet, H. *Natl. Stand. Ref. Data. Ser., Natl. Bur. Stand.* **1971**, *No. 37*.
(28) Evans, M. V.; Lord, R. C. *J. Am. Chem. Soc.* **1960**, *82*, 1876.
(29) Rossi, M.; Golden, D. M. *J. Am. Chem. Soc.* **1979**, *101*, 1230.
(30) Houle, F. A.; Beauchamp, J. L. *J. Am. Chem. Soc.* **1978**, *100*, 3290.
(31) McLoughlin, R. G.; Morrison, J. D.; Traeger, J. C. *Org. Mass Spectrom. 1979*, *14*, 104.
(32) Bombach, R.; Dannacher, J.; Stadelmann, J.-P. *Chem. Phys. Lett.* **1983**, *95*, 259.